CLM-P799

CLM-P799

UKAEA

Preprint

STABILITY OF IDEAL AND RESISTIVE INTERNAL KINK MODES IN TOROIDAL GEOMETRY

R. J. HASTIE
T. C. HENDER
B. A. CARRERAS
L. A. CHARLTON
J. A. HOLMES

CULHAM LABORTORY
Abingdon Oxfordshire
1987

CLM-P.799

STABILITY OF IDEAL AND RESISTIVE INTERNAL KINK MODES IN TOROIDAL GEOMETRY

R.J. Hastie, T.C. Hender,

Culham Laboratory, Abingdon, Oxon, OX14 3DB, UK.

(EURATOM/UKAEA Fusion Association)

B.A. Carreras, L.A. Charlton and, J.A. Holmes,

Oak Ridge National Laboratory, Oak Ridge, TN 37831 U.S.A.

Abstract

The stability of the ideal and resistive m = 1 internal modes is investigated for Tokamak equilibria having a variety of different q(r) profiles, including non-monotonic q(r) with multiple q = 1 surfaces. Detailed comparisons between analytic theory and numerical results from a linear toroidal mhd code are presented. Particular attention is paid to the study of equilibria which are near marginal stability.

(Submitted for publication in Physics of Fluids)

November, 1986

Introduction

Theoretical investigations of the internal disruptions (sawtooth behaviour) observed in most Tokamak discharges have concentrated on three separate aspects of the phenomenon:- (i) the reconnection[1-6] occurring during the non-linear phase of the m = 1, n = 1 kink instability; (ii) the simulation by transport codes [3,4] of the slow evolution of the discharge which returns it to a kink-unstable state, resulting in the cyclic behaviour observed; and (iii) the establishment of marginal stability criteria for the internal kink mode (resistive as well as ideal) and studies of linear growth [7-12] near to marginal stability. Without the third ingredient the transport simulations lack credibility because they assume the plasma reconnects when some arbitrary criterion is satisfied, and the non-linear reconnection studies lack credibility because they start from a strongly unstable equilibrium.

Recent sawtooth simulations [13,14] have employed reduced fluid equations which follow both the fast Alfvenic time scales and the transport time scale. The equations include electron thermal transport both along and across the magnetic field as well as resistivity. These simulations extend the earlier work of Sykes and Wesson[5] and have been very successful in producing cyclical reconnecting behaviour. However, the geometry is cylindrical, and as is well known the stability properties of the internal kink mode are quite different in cylindrical and toroidal geometry.[8] The conditions under which each thermal collapse is triggered may therefore be rather different in this simulation from that holding in a real Tokamak discharge.

Another difficulty encountered in sawtooth simulations, concerns the very fast collapse time frequently observed in large Tokamaks (100μ sec in JET). As noted by Wesson[7] this collapse time is at variance with the estimate given by Kadomtsev, and is difficult to reconcile with any mechanism involving a transport induced evolution through a linear stability boundary, be it of an ideal or a resistive mode. If such a mechanism is responsible for the temperature collapse, an exceedingly sharp stability boundary must be involved: sharp, that is, in the sense of large growth rates being possible for equilibrium parameters close to marginality.

A knowledge of linear stability criteria, and of linear growth rates near marginal stability, is therefore an important ingredient in understanding sawtoothing in Tokamaks. An important contribution in this field is the Toroidal calculation of the ideal mhd energy δW by Bussac et al[8] (subsequently presented in more detail[15-17]). From the later paper by Bussac et al[10] one can obtain analytic expressions for the linear growth rate of the internal kink mode in a resistive plasma as well as in the ideal limit $S \to \infty$ (where S is the magnetic Reynolds number). These results are limited in several ways, all of which may be relevant to understanding sawtoothing. These are:-

(i) The analysis assumes an aspect ratio expansion of the equilibrium, and orders $\beta \sim \varepsilon^2$, where ε is the inverse aspect ratio.

(ii) Only q(r) profiles (where q is the safety factor) having a single q=1 radius, are considered.

(iii) In the inner region, $r \leq r_1$ where $q(r_1) = 1$, the ordering $|q - 1| >> \varepsilon$ is assumed.

It is the purpose of this paper to remove these limitations and to establish the internal kink stability properties of Tokamaks for a variety of q(r) profiles, including non-monotonic q(r), at finite as well as large aspect ratio. We devote particular attention to identifying marginally stable equilibrium configurations, and to evaluating growth rates close to marginality, for both the ideal and resistive internal kink modes. Detailed quantitative comparisons are made between the computational results obtained from a linear toroidal resistive mhd code (FAR)[18,19] and analytic results.

The structure of the paper is as follows:- in section 2 we summarise the analytic theory for ideal internal kink modes when a single $q = 1$ surface is present in the plasma, and extend it to cases for which two $q = 1$ radii are present. In section 3 results from analytic theory are compared with numerical growth rates obtained from the FAR code. In section 4 numerical results are presented for tight aspect ratio devices, strong shaping, and very low shear profiles. These calculations include examples which model the measured q profiles in ASDEX[20] and in TEXTOR[21]. Many of the calculations are for equilibria consistent with JET. These cases are strictly beyond the regime of validity of the analytic theories.

Finally in section 5, the results are summarised, and conclusions on the nature of the sawtooth collapse are drawn.

Section 2

Analytic Theory of Internal Kink Stability

(a) Cases with a single q = 1 surface.

The ideal mhd toroidal stability problem was considered for a large aspect ratio torus by Bussac et al[8] and the effect of shaping was analysed by Edery et al.[22] Shaping effects decouple from toroidal effects in the large aspect ratio limit, so that the combined effects are additive. For an equilibrium of circular cross section the energy integral δW, after minimisation, is given by

$$\delta W = 2\pi^2 R B_o^2 |\xi|^2 \frac{r_1^4}{R^2} \delta W^{(T)} \tag{1}$$

where

$$\delta W^{(T)} = \frac{\{8s(b-c)+\frac{9}{4}(b-1)(1-c)-6(b-1)(c+3)(\beta_p+s)-4(c+3)(b+3)(\beta_p+s)^2\}}{16(b-c)} \tag{2}$$

$$\text{where } s = \int_o^{r_1} \frac{dr}{r_1}\left(\frac{r}{r_1}\right)^3\left(\frac{1}{q^2}-1\right) \tag{3}$$

$$\beta_p = -\frac{2}{B_p^2(r_1)} \int_o^{r_1} \frac{dp}{dr}\left(\frac{r}{r_1}\right)^2 dr \tag{4}$$

with B_p the poloidal field strength and r_1 the radius at which $q(r) = 1$. The quantities b and c in $\delta W^{(T)}$ are the values of the logarithmic derivatives

$$b = \frac{r_1}{\xi}\frac{d\xi}{dr}\Big|_{r_1-} \quad ; \quad c = \frac{r_1}{\xi}\frac{d\xi}{dr}\Big|_{r_1+} \tag{5}$$

obtained on integrating the m = 2 Euler equation

$$\frac{d}{dr}\left(r^3\left(\frac{1}{q} - \frac{1}{m}\right)^2\frac{d\xi}{dr}\right) - (m^2 - 1)\left(\frac{1}{q} - \frac{1}{m}\right)^2 r\xi = 0 \tag{6}$$

from the axis (with regular boundary condition there) to give b and from the q = 2 surface, (or the plasma boundary, if there is no q = 2 surface within the plasma) to give c.

An important feature of the toroidal effects [8] is that the cylindrical contribution to δW is identically cancelled out for an n = 1, m = 1 mode in toroidal geometry. It follows that if the value of the ideal MHD energy, δW, is important in determining the trigger for internal disruption and reconnection, cylindrical simulations must give incorrect results.

To obtain the linear growth rate of either the ideal MHD mode or the resistive kink mode, the above calculation of δW must be supplemented by a theory of the singular layer.

In the case of the ideal mode the growth rate may be obtained by equating the kinetic energy, K

$$K = \frac{\gamma^2}{2}\rho\int|\xi|^2 d^3x \tag{7}$$

to the potential energy available for instability, $(-\delta W)$.[23] Because of the inertial layer at r_1, K is dominated by the contributions from ξ_θ^2 and ξ_ϕ^2 in the inertial layer, where

$$\xi_\theta \sim -\, i\frac{d\xi_r}{dr}$$

$$\xi_\phi \sim \quad 2\sin\theta\,\frac{d\xi_r}{dr} \tag{8}$$

while the discontinuity at the singular layer is resolved by the inertia, and one finds

$$\frac{d}{dr}\left[\left\{3\,\frac{\gamma^2}{\omega_A^{\,2}} + \left(\frac{1}{q} - 1\right)^2\right\}\frac{d\xi_r}{dr}\right] = 0 \tag{9}$$

with $\omega_A = V_A/R$ and V_A the Alfvén velocity.

The factor 3 appearing in equation (9) is the inertial enhancement factor $M \simeq 1 + 2q^2$ found by Glasser, Greene and Johnson [24] in toroidal geometry. To obtain the correct linear growth one must add the field line bending modification to the potential energy which comes from the layer. This is given by

$$\delta\bar{W} = \frac{1}{2}\int d^3x\; B_o^{\,2}\left(\frac{1}{q} - 1\right)^2\left|\frac{d\xi_r}{dr}\right|^2. \tag{10}$$

At marginal stability this contribution vanishes, but when eqn (9) is used to give the layer solution a finite contribution is obtained.

Finally, equating $K = -\left[\delta W + \delta\bar{W}\right]$ one obtains the linear growth rate

$$\left\{ \int_{-\infty}^{\infty} \frac{dx}{3\left(\frac{\gamma^2}{\omega_A^2}\right) + (q - 1)^2} \right\}^{-1} = - \frac{r_1^2}{R^2} \delta W^T \qquad (11)$$

where $x = (r - r_1)/r_1$ is the local radial variable.

Several cases can now be distinguished:-

(i) Monotone $q(r)$: $q(r_1) = 1$ and $q'(r_1) \neq 0$. (Fig. 1a)

$$\frac{\gamma}{\omega_A} = \frac{1}{r_1 q'} \frac{\pi}{\sqrt{3}} \left[-\delta W^{(T)} \right] \frac{r_1^2}{R^2} \qquad (12)$$

(ii) Non-monotone $q(r)$ with a minumum at r_1, $q(r_1) = 1$ and $q'(r_1) = 0$ (Fig. 1b)

$$\frac{\gamma}{\omega_A} = \frac{\pi^{2/3}}{\sqrt{3}} \frac{1}{(r_1^2 q'')^{1/3}} \left[- \frac{r_1^2}{R^2} \delta W^T \right]^{2/3} \qquad (13)$$

(iii) Non-monotone $q(r)$, with $q(r_1) \neq 1$ and $q'(r_1) = 0$ (Fig. 1c)

$$\bar{\gamma}\left[1 + \frac{\delta q}{\bar{\gamma}}\right]^{1/3} = \frac{1}{(r_1^2 q'')^{1/3}} \left[- \pi \frac{r_1^2}{R^2} \delta W^T \right]^{2/3} \qquad (14)$$

where $\bar{\gamma} = \left[\frac{3\gamma^2}{\omega_A^2} + (\delta q)^2\right]^{1/2}$ and $\delta q = q(r_1) - 1 \ll 1$. The above expression (14) is valid for both positive and negative values of δq, provided that

when $\delta q < 0$, $|\delta q|$ does not become large enough for the inertial layer to separate into two layers at the different $q = 1$ radii. For positive δq there is a strong stabilising effect from the field line bending at r_1, and an equilibrium which is unstable when $q_{min} = 1$ (i.e for which δW^T is negative) is marginally stable for

$$\delta q = \frac{1}{2^{1/3}} \frac{1}{(r_1^2 q'')^{1/3}} \left[-\pi \frac{r_1^2}{R^2} \delta W^T\right]^{2/3} \qquad (15)$$

The ideal growth rate peaks for negative δq at $\gamma_{max} = 1.09\ \gamma_0$ with γ_0 the $\delta q = 0$ growth rate. As δq becomes more negative the growth rate decreases, but the single layer theory eventually becomes invalid. These analytic results are compared with computed growth rates in the next section, (Fig.4).

(iv) Monotone $q(r)$ with a point of inflection at r_1: $q(r_1) = 1$

$q'(r_1) = q''(r_1) = 0$

$$\frac{\gamma}{\omega_A} = \frac{1}{\sqrt{3}} \left(\frac{6}{r_1^3 q'''}\right)^{1/5} \left[-\frac{2\pi}{3} \frac{r_1^2}{R^2} \delta W^T\right]^{3/5} \qquad (16)$$

The presence of a point of inflection of q at r_1, therefore, enhances the ideal mhd growth rate ($\gamma \alpha (r_1/R)^{6/5}$) when $\delta W^T < 0$. For $\delta W^T > 0$ the resistive stability of such $q(r)$ profiles is investigated in Sec.4.

(b) The role of resistivity.

In the foregoing estimates of growth rates it has been assumed that $\delta W^T < 0$, i.e. that there is energy available to drive ideal mhd instability. However, even when this is the case it does not follow that the ideal growth rates calculated above are correct. Resistivity may dominate the layer behaviour. To estimate the magnitude of resistive effects we compare the inductive contribution to the parallel electric

field, $\gamma A_{\parallel}$, with the resistive term in the layer $\eta j_{\parallel} \alpha \frac{\eta c^2 A_{\parallel}}{d^2}$ where d is a measure of the layer width.

From this we find that resistivity is negligible if the condition

$$\left(\frac{\gamma}{\omega_A}\right)\left(\frac{d^2}{r_1^2}\right) > S^{-1} \qquad (17)$$

is satisfied.

Here, $S = \omega_A \tau_r$ with $\tau_r = \eta c^2/r_1^2$.

Estimating the layer width d from equation (9) and the growth rates from equations (12) and (13) we find that for $q'(r_1) \neq 0$ inequality (17) becomes

$$S^{-1} < \frac{\pi^3}{\sqrt{3}} \left(r_1 q'(r_1)\right)^{-5} \left(\frac{r_1}{R}\right)^6 \left[-\delta W^{(T)}\right]^3 \qquad (18)$$

while for the non-monotonic case, (ii) with $q_{min} = 1$, it becomes

$$S^{-1} < \pi^{4/3} \sqrt{4/3} \left(r_1^2 q''(r_1)\right)^{-5/3} \left(\frac{r_1}{R}\right)^{8/3} \left[-\delta W^{(T)}\right]^{4/3} \qquad (19)$$

where the layer width is $d/r_1 \approx \sqrt{2}\pi^{1/3} \left(\frac{r_1}{R} \frac{1}{r_1^2 q''}\right)^{2/3} \left(-\delta W^{(T)}\right)^{1/3}$.

Inequality (18) gives the familiar result that resistivity (even with S in the range 10^6 - 10^8) tends to dominate the linear growth of m = 1 modes.

Inequality (19) however, shows that because of the broader inertial layer and larger ideal growth rate the internal kink becomes an essentially ideal mode when the shear vanishes at the q = 1 surface.

When $\delta W^{(T)} > 0$ no ideal instability is possible and a resistive layer theory is required. Coppi et al[9] have given this theory in cylindrical geometry (with $q'(r_1) \neq 0$) and Bussac et al[10] have extended this to toroidal geometry. The dispersion relation is given in reference (10) with diamagnetic and toroidal coupling effects included. In single fluid resistive theory, neglecting coupling to the q = 2 tearing mode, it reduces to

$$\frac{r_1^2}{R^2}\,\delta W^{(T)} + \frac{2}{\pi}(r_1 q')^{3/2}\left[\frac{3\gamma}{\omega_A S}\right]^{1/4}\frac{\mu - 1}{\mu}\,\frac{\Gamma\left(\frac{\mu+5}{4}\right)}{\Gamma\left(\frac{\mu+3}{4}\right)} = 0 \qquad (20)$$

with $\mu = \frac{\sqrt{3}}{rq'}\left(\frac{\gamma}{\omega_A}\right)^{3/2} S^{1/2}$

This yields the ideal mhd growth rate when $\delta W^{(T)} < 0$ and $S \to \infty$, and the familiar $\gamma \propto S^{-1/3}$ scaling when $S < \left|\frac{r_1^2}{R^2}\,\delta W^T\right|^3$. For very large S, very tight aspect ratio or small shear ($q'(r_1) \to 0$) the scaling of γ is modified to the $S^{-3/5}$ of conventional tearing modes. No theory of the resistive layer appears to have been done when $q'(r_1) = 0$, but as we shall see from the numerical results, no unstable m = 1 resistive mode is found when $q(r) \geq 1$ everywhere, provided the rippling modes are excluded.

(c) Equilibria with two q = 1 surfaces.

As noted in the foregoing, the analytic estimate of the growth rate given by equation (14) breaks down when the characteristic layer width d

becomes less than the separation of the two q = 1 radii when $q_{min} < 1$.

The analytic minimisation of δW for two q = 1 radii is similar to the original analysis of Bussac et al. The analysis is outlined in the appendix, where the following expression for δW is obtained.

$$\delta W = 2\pi^2 R B_0^2 \left\{ (\xi - \bar{\xi})^2 \frac{r_1^4}{R^2} \delta W_1 + \bar{\xi}^2 \frac{r_2^4}{R^2} \delta W_2 + \bar{\xi}(\xi - \bar{\xi}) \frac{r_1^4}{R^2} \delta W_3 \right\} \qquad (21)$$

with r_1 the radius of the first and r_2 the radius of the second q = 1 surface, ξ the amplitude of the 'top-hat' m = 1 eigenfunction in $[0, r_1]$ and $\bar{\xi}$ the amplitude in $[r_1, r_2]$. The expressions for δW_1, δW_2 and δW_3 are given in the appendix. They depend on the quantities

$$s_j = \int_o^{r_j} \frac{dr}{r_j} \left(\frac{r}{r_j}\right)^3 \left(\frac{1}{q^2} - 1\right) , \quad j = 1,2 \qquad (22)$$

$$\text{and } \beta_{pj} = - \frac{2}{B_p^2(r_j)} \int_o^{r_j} \frac{dp}{dr} \left(\frac{r}{r_j}\right)^2 dr , \quad j = 1,2 \qquad (23)$$

which are obvious generalisations of the single surface case.

The ideal growth rates, and eigenfunctions (ratio of ξ to $\bar{\xi}$) of the two possible ideal modes are also calculated in the appendix.

The results are

$$\frac{\gamma}{\omega_A} = \frac{\pi}{\sqrt{3}} \frac{1}{2DE} \left[(AE+CD) \pm \sqrt{(AE+CD)^2 + (B^2-4AC)DE} \right] \qquad (24)$$

and

$$\frac{\xi}{\bar{\xi}} = 1 + \frac{r_2}{r_1}\frac{1}{BE}\left[-(AE-CD) \pm \sqrt{(AE+CD)^2 + (B^2-4AC)DE}\right] \qquad (25)$$

where $A = \frac{r_2^2}{R^2}\delta W_2$, $B = \frac{r_1^3}{R^2 r_2}\delta W_3$, $C = \frac{r_1^2}{R^2}\delta W_1$,

$$D = |r_2 q'(r_2)|, \quad E = |r_1 q'(r_1)|$$

3. Comparison of analytic and numerical results.

In this section we demonstrate the very close agreement which exists between the aspect ratio expansion analytic techniques presented in section 2, and computational results using a modified version of the FAR code.[18] The modified FAR code[19] solves the linear compressible (or incompressible) resistive mhd equations in full toroidal geometry, with no ordering assumptions. The double equations of state, $\frac{dp}{dt} = 0$, and $\nabla.(\underline{v}/R^2) = 0$ employed in the original FAR code [18] have therefore been replaced by the adiabatic equation of state or, in the incompressible case, by $\nabla.\underline{V} = 0$. As a result the localised resistive pressure-driven modes which appeared in earlier $m = 1$ simulations using the original FAR code,[18] and in simulations with reduced equations using the RST code,[25] do not appear at finite β.

In all other respects the new version of FAR is identical to the original code as described in ref. (18). As input to the FAR code the flux coordinates are computed from numerical solution of the Grad-Shafranov equation.

I. Monotonic q(r)

Fig.2 shows the variation of ideal mhd growth rate with β for monotonic $q(r) = 0.9(1+r^2)$. The aspect ratio $A = 10^2$ and the pressure profile is a parabolic function of r, the flux coordinate used in ref.8. For this comparison the logarithmic derivatives b and c of equation (5) were evaluated numerically and found to be 1.15 and - 2.02 respectively. The code was run incompressibly with resistivity set to zero. As predicted analytically $\gamma \propto \beta^2$ and close agreement exists between computational and analytic results.

Fig.3 shows the growth rate of the resistive mode as a function of the magnetic Reynolds number S, for the same equilibrium as Fig.2, but at zero beta. The comparison is now with the analytic prediction taken from equation (20). Within the range of S values investigated the dispersion relation is effectively $\mu = 1$, so that $\delta W^{(T)}$ plays no role. The growth rate scales as $S^{-1/3}$. At even higher S a transition to $S^{-3/5}$ behaviour should occur (probably beyond $S = 10^{12}$ for this case). This transition is demonstrated for an equilibrium of tight aspect ratio in section 4.

II. Non-monotonic q(r).

In Fig.4 we compare the ideal mhd growth rates computed from the FAR code with those calculated analytically for the non-monotonic profile

$$q = q_{min} + 0.2\ (1 - 4r^2)^2$$

at zero beta and A = 10.

The solid curve is that given by equation (24) which should be valid whenever two separate inertial layers are present. The broken curve is

evaluated from equation (14) which should apply when only one inertial layer is present. A striking feature is the very sharp stability boundary close to $q_{min} = 1$. Results are also shown in Fig.4 from the compressible FAR code. At zero beta the sound waves no longer propagate in a compressible formulation and the inertial enhancement factor $M \simeq 1$ (as opposed to $M \simeq 1+2q^2$ when the sound waves propagate faster than the mode grows). Thus the compressible and incompressible growth rates should and do differ by the factor $\sqrt{(1+2q^2)} = \sqrt{3}$.

The spatial dependence of the radial displacement eigenfunction is shown in Fig. 5 for various values of q_{min}. The transition from one inertial layer when $q_{min} = 0.99$, to two separate layers when $q_{min} \lesssim 0.97$ is apparent. In the cases with two distinct layers the ratios of the constant values for the eigenfunction in $[o, r_1]$ and $[r_1, r_2]$ are in good agreement with the analytic prediction in eq. (25). Fig.6 shows the variation of growth rate with aspect ratio for this case with $q_{min} = 1.0$, with close agreement again between analytic and computed results.

The non-monotonic class of profiles studied here includes a marginally stable equilibrium (for ideal mhd modes). This remains true when finite resistivity is introduced and will be demonstrated for JET like equilibria in the next section.

Fig.7 shows a comparison of analytic (eq. 13) and computed growth rates as functions of β, for the non-monotonic $q(r) = 1 + \Delta q(1 - (\frac{r}{r_1})^2)^2$ with $\Delta q = .1$, $r_1 = 0.33$, and an aspect ratio $A = 10$. In this case the term in δW which is linear in β is weakly stabilising but is rapidly dominated by the quadratic term as β is increased. Thereafter the growth rate γ scales as $\beta^{4/3}$.

The remarkable quantitative agreement found in the foregoing comparisons demonstrates that the analytic, large aspect ratio, theory provides an extremely valuable framework for understanding the varied scalings of linear growth rate with S, β, ε etc, which emerge when different equilibrium q(r) profiles are investigated.

4. Numerical Results.

In this section we extend the results of the previous section by computing growth rates of ideal and resistive mhd modes in various equilibria for which the analytic theory should be expected to break down; namely equilibria of small aspect ratio (A<3), strongly shaped cross section, or very flat q(r) within $[0,r_1]$, or very low shear at the q = 1 surface.

Fig.8 shows the transition from resistive kink behaviour ($\gamma \propto S^{-1/3}$) to the more slowly growing tearing mode (reconnecting mode[12], $\gamma \propto S^{-3/5}$) at high values of S, for the profile $q(r) = 0.9\left(1+\left(\frac{r}{0.65}\right)^4\right)^{1/2}$ at A = 1.4. (We are forced to use this very tight aspect ratio to recover tearing mode behaviour even for the high S values ($\sim 10^8$) used.) In the high S, or tearing regime, this mode should be sensitive to the stabilising effect of favourable average curvature.[24] This effect is however rather weak at the q = 1 surface since the D_R of ref.(24) is much reduced there.

Fig.9 contrasts the resistive kink mode eigenfunction corresponding to Fig.3 with the very localised tearing mode eigenfunction corresponding to Fig.8, (at $S = 10^7$).

Fig.10 shows the growth rate of the m = 1 mode at the JET aspect ratio of A = 2.5 for the non-monotonic $q(r) = q_{min} + 0.1(1 - 8r^2+16r^4)$,

and several values of S. The equilibria in this case have a circular boundary. The behaviour of γ is qualitatively the same as that found at large aspect ratio, (Fig.4), and a notable feature is again the sharp stability boundary. In this case when $q_{min} \geq 1$ the growth rates are almost independent of S, with very weak resistive damping when $q_{min} > 1$ (Fig.11). As noted in the previous section this shows that the non-monotonic profile considered is marginally stable to both ideal and resistive m = 1 instability when q_{min} is slightly above unity. For $q_{min} < 1$ the usual $\gamma \propto S^{-1/3}$ scaling of resistive kink modes is also displayed in Fig.11.

Fig.12 shows the destabilising effect of β for the previous case, with $q_{min} = 1$, while Fig.13 shows a new important <u>destabilising</u> effect from triangular shaping. This last result is in qualitative agreement with analytic theory. Previous results[22] have indicated that triangular, quadrangular and high order shaping is stabilising for internal kink modes, but in these calculations monotonic q(r) was assumed. The present result shows that this stabilising effect is profile dependent and can be reversed for non-monotone q(r).

Recently, Wesson[7] has suggested a sawtooth model which is quite different from the original Kadomtsev model, and which has as its crux the assumption of an 'ultra-flat' q(r) profile for $0 < r \leq r_1$. This assumption is supported by both the measurements on ASDEX[20] and by transport code simulations which, once such a flat q is established, tend to show very small deviations from it. Fig.14 shows the growth rate as a function of q on axis for an 'ultra-flat' profile

$$q = q_o \left[1 + \left(\frac{r}{0.462}\right)^{12}\right]^{1/6}$$

at the JET aspect ratio A = 2.5, and central beta of 2%. Various values of S are shown, but it is clear that the unstable mode is essentially ideal near $q_o \sim 1$. For $q_o \geq 1.02$ the 'm = 2' tearing mode becomes unstable: the transition from an m = 1 to an m = 2 mode being clear in the energy spectra of the eigenmodes. The sharp ideal stability boundary similar to that found for non-monotone q(r) is again evident. Growth rates calculated from the compressible FAR code are also shown in Fig.14. For this finite β equilibrium sound propagation along the magnetic field is faster than mode growth so that the compressible and incompressible results are in good quantitative agreement.

In Fig.15 the dependence of the linear growth on β is shown for the same case as Fig.14($S = 10^6$), and in Fig.16 the eigenfunctions are compared for various values of β_o and q_o. In all cases the eigenfunctions extend out to a significant radius, and in addition those closest to marginal stability show the rounded feature observed in the reconstructed flows using soft x-ray data[26].

Fig.17 shows a similar plot of γ against q_o for a somewhat less flat $q(r) = q_o\left[1+\left(\frac{r}{.46}\right)^4\right]^{1/2}$ with all other parameters identical to Fig.14. The increasingly sharp ideal stability boundary as the shear within the q = 1 radius decreases is evident when Figs.14 and 17 are compared.

Experimental measurements on TEXTOR[21] have produced evidence of somewhat different profiles of the safety factor and longitudinal current. In TEXTOR measurements of the poloidal magnetic field indicate an axial value of the safety factor $q_0 \leq 0.7$, with a point of inflection in the current $J_\parallel(r)$ and somewhat reduced shear at the q = 1 surface. For such an equilibrium the original Bussac et.al. theory of ideal [8] and resistive [10] stability is valid. This theory predicts that, at large

aspect ratio, the ideal mhd mode should be stable below some critical β-value, while the resistive m = 1 mode should be unstable (whatever the β).

Since the effective Δ' for driving the resistive m = 1 mode in toroidal geometry[10] is $[q'(r_1)]^2/[\varepsilon_1^2 \delta w^{(T)}]$ for a large aspect ratio device, it is of interest to investigate what might be gained by modifying the current profile to remove the shear completely at $r_1 (q'(r_1) \to 0)$ in a tight aspect ratio torus. To study the general properties of profiles of this class we adopt the simple parametrisation

$$q = 0.6 + 2.2r^2 - 2.2(r^2 - r_1^2)e^{-100(r^2 - r_1^2)^2} \quad \text{with } r_1 = .426.$$

so that $q'(r_1) = q''(r_1) = 0$ with $q(r_1) = 1$.

Results from the FAR code for this equilibrium profile (with $\beta \equiv 0$) are shown in Fig.18 where a strong stabilising trend is evident as aspect ratio, A, is reduced. Surprisingly, for a force free equilibrium, the mode becomes overstable at small aspect ratio. Overstability may (as in the favourable curvature stabilisation[24] of conventional tearing modes) be symptomatic of a stabilising mechanism within the layer which could yield absolute stability below some critical value of A. This is difficult to establish computationally and remains a conjecture.

5. Discussion and Conclusions

A key ingredient in understanding, and possibly controlling the internal disruptions in Tokamaks is an understanding of the stability boundary which is crossed at the instant of the fast temperature crash. An important clue is provided by the experimental observation that the phase inversion radius of the temperature collapse which is usually

interpreted as the radius of the q = 1 surface, is not small. The marginal q(r) profiles therefore appear to pass through, or close to, unity at a finite distance, r_1 from the axis of the discharge.

As a result of the calculations presented here we can distinguish three distinct classes of q(r) profile which possess this property, and can be marginally stable to m = 1 modes. These are:-

(i) non-monotonic q(r) with a minimum value close to unity at $r = r_1$

(ii) ASDEX-like, or ultra-flat q(r) profiles which are close to unity over the whole region $[0, r_1]$

(iii) Monotonic q(r) profiles for which q_0 is well below unity, $q(r_1) = 1$ and r_1 is a point of inflection for q, or at least a point of weak shear.

Examples of each of these profiles have been analysed for ideal and resistive growth close to marginal stability, and earlier analytic theory[8] has been extended to provide a framework for understanding computational results from the initial value code FAR. Remarkable agreement has also been found in comparing analytic and computed growth rates.

Amongst the new results presented here, are the observations that

(i) very sharp stability boundaries can be found when a critical q value determines stability. Examples are given for 'ultra flat' and non-monotonic q profiles.

(ii) $S^{-1/3}$ scaling of linear growth rates is not found for any of the profiles (i) - (iii) above, close to marginal stability.

(iii) Triangular shaping of the plasma cross-section can be destabilising. Its effect is dependent on the q(r) profile.

(iv) Equilibria with axial q values well below unity have been found which may be stable to resistive as well as ideal mhd m = 1 modes, in a tight

aspect ratio torus. Overstability of the mode makes the determination of a stability boundary in A difficult.

Many of the features of the sawtooth in smaller Tokamaks were explained by the model of Jahns et. al.[27] which invoked island growth of the resistive kink mode. In particular the precursor oscillations, and their growth rates, agreed with the model proposed. In larger tokamaks, such as JET, however, precursor oscillations are not usually observed[28] in conditions of constant current. In addition the initial plasma displacement in the sawtooth collapse is too fast (100 μsec in JET[28]) for the model of ref (27). This suggests that the steep, ideal mhd, stability boundaries apparent in Figs.(4) and (10) might be involved. We can calculate the initial time dependence to be expected as an equilibrium evolves resistively through such a boundary. Assuming a time dependence of the q profile such that

$$q = q(r)\left[1 - \frac{t}{\tau_\eta}\right], \qquad \text{with } \tau_\eta = \frac{r_1^2}{\eta c^2}$$

and using equation (14) for the growth rate (for a non-monotonic $q(r)$ with $(q_{min} - 1) = \delta q$) we find that initially the mode growth is given by $\exp\left(t/\tau_H\right)^{3/2}$, with the hybrid time τ_H defined by

$$\tau_H = \left(3\tau_A^2\tau_\eta/\delta q_c\right)^{1/3} \tag{26}$$

where δq_c is the value of δq at the stability boundary. Thus, even though the mode is an ideal mhd instability, the resistive evolution of q introduces an $\eta^{1/3}$ into the time scale. Estimating this hybrid growth

time for JET parameters, we find $\tau_H \sim 300$ μsec which is still a little too long to account for the experimental observations. To understand the fast time scales involved, it therefore appears that theory must look to non-linear, or kinetic-theory phenomena.

To understand the nature of the internal disruptions in Tokamaks it is necessary to study the non-linear evolution of the m = 1, n = 1 kink mode. The present paper suggests a number of equilibrium q(r) profiles which could be marginally stable in linear theory, and which therefore are appropriate initial states for such non-linear studies. Because of the considerable differences in these q profiles a wide variety of non-linear behaviour is to be expected, with the classic Kadomtsev reconnection as one possibility. Such studies are under way using a non-linear version of the FAR code, and will form the basis of a future paper.

Acknowledgement

This work was supported in part by United States Office of Fusion Energy under contract no. DE-AC05-840R21400 with Martin Marietta Energy Systems, Inc. One of us (T.C.H.) was supported in part by a task agreement between the JET Joint Undertaking and Culham Laboratory.

Appendix A

The ideal mhd theory of Bussac et al[8] can be readily extended to the case with two distinct radii at which q is unity. Denoting these by r_1 and r_2, we follow refs.(8) and (15) in expanding the ideal energy integral δW in powers of the inverse aspect ratio, for a large aspect ratio equilibrium, with circular plasma cross section and poloidal beta of order unity. Using the straight field line coordinates of ref.(8) and (17), r, θ, ϕ

$$r^2 = 2 R_o \int_o^{\psi} \frac{q}{I} d\Psi \qquad \text{A.1}$$

$$\theta = \frac{I}{q} \int_o^{\ell} \frac{d\ell}{R^2 B_p} \qquad \text{A.2}$$

and ϕ is the axisymmetric angle. In (A.1) and (A.2) Ψ is the poloidal flux function, and the magnetic field is given by

$$\underset{\sim}{B} = \nabla\Psi \times \nabla\phi + I(\Psi)\nabla\phi$$

and ℓ measures arc-length along $\underset{\sim}{B}$.

In lowest order of the aspect ratio expansion, one finds $\delta W_o = 0$ provided ξ_o is chosen to satisfy

$$\frac{\partial}{\partial r}\left(r\xi_{ro}\right) + \frac{\partial}{\partial\theta}\xi_{\theta o} = 0 \qquad \text{A.3}$$

where $\underset{\sim}{\xi}_o \propto e^{i(m\theta - n\phi)}$ with m = n = 1.

In second order, $\underset{\sim}{\xi}_1$ is also required to satisfy (A.3) and

$$\delta W_2 = 2\pi^2 R_o B_o^2 \int r\, dr\, \{(\frac{1}{q} - 1)^2 |r \frac{d\xi_{ro}}{dr}|^2\} \qquad A.4$$

This is minimised by the choice

$$\left.\begin{aligned} \xi_{ro} &= \xi_o,\ 0 \leq r < r_1 \\ &= \bar{\xi}_o,\ r_1 < r < r_2 \\ &= 0,\ r_2 < r \leq a \end{aligned}\right] \qquad A.5$$

when $\delta W_2 = 0$.

The relative magnitudes of the 'top-hat' solutions ξ_o and $\bar{\xi}_o$ are arbitrary at this stage.

In fourth order, after minimising with respect to $\underset{\sim}{\xi}_2$ the second order correction to the m = 1 component, and with respect to the m = 0 part of $\underset{\sim}{\xi}_1$, one obtains

$$\delta W_4 = \delta W_4(0,r_1) + \delta W_4(r_1,r_2) + \delta W_4(r_2,a)$$

where

$$\frac{\delta W_4(o,r_1)}{2\pi^2 R_0 B_0^2} = \xi_0^2 \frac{r_1^4}{R^2}\left\{\frac{1}{2}s_1 - \frac{3}{4}(s_1+\beta_{p1})^2 - \frac{9}{8}(s_1+\beta_{p1}) + \frac{9}{64}\right\}$$

$$+ \frac{3}{2}\xi_0\xi_1(r_1)\frac{r_1^3}{R}(s_1 + \beta_{p1} - \frac{1}{4}) + \frac{1}{4}r_1^3\,\xi_1\xi_1'\Big|_{r_1} \qquad \text{A.6}$$

$$\frac{\delta W_4(r_1,r_2)}{2\pi^2 R_0 B_0^2} = \bar{\xi}_0^2 \frac{r_2^4}{R^2}\left\{\frac{1}{2}s_2 - \frac{3}{4}(s_2+\beta_{p2})^2 - \frac{9}{8}(s_2+\beta_{p2}) + \frac{9}{64}\right\}$$

$$- \bar{\xi}_0^2 \frac{r_1^4}{R^2}\left\{\frac{1}{2}s_1 - \frac{3}{4}(s_1+\beta_{p1})^2 - \frac{9}{8}(s_1+\beta_{p1}) + \frac{9}{64}\right\}$$

$$+ \frac{3}{2}\frac{r_2^3}{R}\bar{\xi}_0\bar{\xi}_1(r_2)\left[s_2+\beta_{p2} - \frac{1}{4}\right] - \frac{3}{2}\frac{r_1^3}{R}\bar{\xi}_0\bar{\xi}_1(r_1)\left[s_1+\beta_{p1} - \frac{1}{4}\right]$$

$$+ \frac{1}{4}r_2^3\,\bar{\xi}_1\bar{\xi}_1'\Big|_{r_2} - \frac{1}{4}r_1^3\,\bar{\xi}_1\bar{\xi}_1'\Big|_{r_1} \qquad \text{A.7}$$

$$\frac{\delta W_4(r_2,a)}{2\pi^2 R_0 B_0^2} = -\frac{1}{4}r_2^3\,\tilde{\xi}_1\tilde{\xi}_1'\Big|_{r_2} \qquad \text{A.8}$$

where

$$s_j = \int_0^{r_j} \frac{r^3 dr}{r_j^4}\left(\frac{1}{q^2} - 1\right) \qquad j = 1,2$$

$$\beta_{pj} = \frac{2}{B_p^2(r_j)} \int_0^{r_j} dr \left(-\frac{dp}{dr}\right) \frac{r^2}{r_j^2} \qquad j = 1,2$$

and $\xi_1(r)$, $\bar{\xi}_1(r)$, $\tilde{\xi}_1(r)$ are all solutions of the homogeneous, m = 2 Euler-equation

$$\frac{d}{dr}\left[r^3\left(\frac{1}{q} - \frac{1}{2}\right)^2 \frac{d\xi_1}{dr}\right] - 3r\left(\frac{1}{q} - \frac{1}{2}\right)^2 \xi_1 = 0 \qquad \text{A.9}$$

Since the full m = 2 solutions in the three regions are given by

$$\xi^{(m=2)} = \xi_1(r) - \xi_0\left(\Delta' + \frac{1}{2}\frac{r}{R}\right) \quad \text{in} \quad [0, r_1]$$

$$\xi^{(m=2)} = \bar{\xi}_1(r) - \bar{\xi}_0\left(\Delta' + \frac{1}{2}\frac{r}{R}\right) \quad \text{in} \quad [r_1, r_2)$$

$$\xi^{(m=2)} = \tilde{\xi}_1(r) \quad \text{in} \quad [r_2, a]$$

continuity of $\xi^{(m=2)}$ requires that

$$\xi_1(r_1) - \xi_0\left(\Delta' + \frac{1}{2}\frac{r}{R}\right)_{r_1} = \bar{\xi}_1(r_1) - \bar{\xi}_0\left(\Delta' + \frac{1}{2}\frac{r}{R}\right)_{r_1} \qquad \text{A.10}$$

and $$\tilde{\xi}_1(r_2) = \bar{\xi}_1(r_2) - \bar{\xi}_0\left(\Delta' + \frac{1}{2}\frac{r}{R}\right)_{r_2} \qquad \text{A.11}$$

In addition $\xi_1(r)$ must be regular as $r \to 0$, and $\tilde{\xi}(r)$ must be small at the $q = 2$ surface if that falls within the plasma, or $\tilde{\xi}_1(a)$ must vanish if $q_a < 2$.

In the above equations $\Delta(r)$ is the Shafranov shift, so that

$$\Delta'(r_1) = \frac{r_1}{R}\left(s_1 + \beta_{p1} + \frac{1}{4}\right),$$

$$\Delta'(r_2) = \frac{r_2}{R}\left(s_2 + \beta_{p2} + \frac{1}{4}\right).$$

To proceed with the minimisation of δW_4, we choose to represent $\bar{\xi}_1(r)$, which is a solution of equation (A.9), by a linear superposition of $\xi_1(r)$ and $\tilde{\xi}_1(r)$, the solutions which are regular at $r = 0$ and at the $q = 2$ surface.

Thus writing

$$\bar{\xi}_1(r) = \alpha\xi_1(r) + \beta\tilde{\xi}(r)$$

the two continuity relations (A.10) and (A.11) are used to eliminate α and β. The energy integral may now be expressed in terms of ξ_0, $\bar{\xi}_0$ and two quantities characterising the magnitude of the $\xi_1(r)$ and $\tilde{\xi}_1(r)$ solution ($\xi_1(r_1)$ and $\tilde{\xi}_1(r_2)$ say), together with six quantities which characterise the solutions ξ_1 and $\tilde{\xi}_1$. These quantities are:-

$$b = \frac{r_1\xi_1'(r_1)}{\xi_1(r_1)} \qquad c = \frac{r_2\xi_1'(r_2)}{\xi_1(r_2)} \qquad d = \frac{r_1\tilde{\xi}_1'(r_1)}{\tilde{\xi}_1(r_1)}$$

$$e = \frac{r_2 \tilde{\xi}_1'(r_2)}{\tilde{\xi}_1(r_2)} \qquad f = \frac{\tilde{\xi}_1(r_1)}{\tilde{\xi}_1(r_2)} \qquad g = \frac{\xi_1(r_2)}{\xi_1(r_1)}$$

Thus

$$\delta W_4 = \delta W_4[\xi_0,\ \bar{\xi}_0,\ \xi_1(r_1),\ \tilde{\xi}_1(r_2);\ \ b,\ c,\ d,\ e,\ f,\ g,\ s_j,\ \beta_{pj}]$$

The next step is to minimise δW_4 with respect to ξ_1 and $\tilde{\xi}_1$. These minimisations are algebraic but tediously complicated. The final result is

$$\delta W_4 = 2\pi^2 R\, B_0^2 \{(\xi_0-\bar{\xi}_0)^2 \frac{r_1^4}{R^2}\, \delta W_1 + \bar{\xi}_0^2 \frac{r_2^4}{R^2}\, \delta W_2 + \bar{\xi}_0(\xi_0-\bar{\xi}_0) \frac{r_1^4}{R^2}\, \delta W_3\} \qquad \text{A.12}$$

with

$$\delta W_1 = \frac{1}{4}\{2s_1 + (b+3)(\beta_{p1}+s_1)^2 + \frac{3}{2}(b-1)(\beta_{p1}+s_1) + \frac{9}{16}(b-1)$$

$$- \frac{1}{\alpha}\frac{(e-c)}{(d-b)}\left[(b+3)(s_1+\beta_{p1}) + \frac{3}{4}(b-1)\right]^2\} \qquad \text{A.13}$$

$$\delta W_2 = \frac{1}{4}\{2s_2 - (e+3)(\beta_{p2}+s_2)^2[1 + (e+3)/\alpha] - \frac{3}{2}(e+3)(\beta_{p2}+s_2)[1+(e-1)/\alpha]$$

$$+ \frac{9}{16}(1-e)[1+(e-1)/\alpha]\} \qquad \text{A.14}$$

$$\delta W_3 = \frac{1}{2}\{2s_1 - 3(\beta_{p1}+s_1) - [(e+3)(\beta_{p2}+s_2) + \frac{3}{4}(e-1)][(b+3)(\beta_{p1}+s_1) + \frac{3}{4}(b-1)]$$

$$\times \frac{1}{2\alpha}\frac{r_2}{r_1}\frac{[(d-b)f+(e-c)g\ r^2{}_2/r^2{}_1]}{(d-b)fg}\} \qquad \text{A.15}$$

$$\alpha = \frac{(e-c)fg}{(1-fg)} - \frac{1}{4}\frac{r_1^2}{r_2^2}\frac{(1-fg)}{(d-b)fg}\left[\frac{(d-b)f}{(1-fg)} + \frac{(e-c)g}{(1-fg)}\frac{r_2^2}{r_1^2}\right]^2 \qquad \text{A.16}$$

The necessary and sufficient condition for ideal mhd m = 1 stability can now be expressed as

(i) $\delta W_1 > 0$

and

(ii) $\delta W_3 > 0$ A.17

and

(iii) $\left(\frac{r_2}{r_1}\right)^8 (\delta W_2)^2 - 4\delta W_1\ \delta W_3 < 0.$

If any one of these three inequalities is violated an ideal m = 1 mode is unstable.

The appropriate ideal growth rates and eigenfunctions of unstable modes are obtained by equating the expression (A.12) to the energy

contributions from the two inertial layers at r_1 and r_2, in an anologous way to that discussed in the main text for a single inertial layer. The single surface result (equation (11)) now becomes

$$\frac{(\xi_0 - \bar{\xi}_0)^2}{I_1(\gamma)} + \frac{\bar{\xi}_0^2}{I_2(\gamma)} = - \frac{\delta W_4(\xi_0, \bar{\xi}_0)}{(2\pi^2 R B_0^2)} \qquad \text{A.18}$$

where $I_j(\gamma) = \int_{-\infty}^{\infty} \frac{dx}{\left[3 \frac{\gamma^2}{\omega_A^2} + [r_j q'(r_j)]^2 x^2 \right]}$

and $\delta W_4 (\xi_0, \bar{\xi}_0)$ is given by A.12.

On solving for γ/ω_A and extremising with respect to the ratio $\xi_0/\bar{\xi}_0$ we obtain the growth rates and eigenfunctions of the ideal modes. It is these results (equations (24) and (25) of the main text) which have been used in the comparison of analytic growth rates with those obtained from the FAR code.

References

1. B.B.Kadomtsev, Soviet J. Plasma Physics, 1, 389 (1975).
2. B.B.Kadomtsev, Plasma Physics and Controlled Nuclear Fusion Research 1976 (Proc. 6th Int. Conf. Berchtesgaden 1976), Vol 1, IAEA, Vienna 555, (1975).
3. V.V.Parail, G.V.Pereverzev, Soviet J. Plasma Phys. 6, 14, (1980).
4. W. Pfeiffer, W., Nucl. Fusion 25, 673, (1985).
5. A.Sykes, J.A.Wesson, Phys. Rev. Lett, 37 140 (1976).
6. B.D.Waddell, M.N.Rosenbluth, D.A.Monticello, R.B.White, Nucl. Fusion 16, 528, (1976).
7. J.A.Wesson, Plasma Physics and Controlled Fusion, 28 243,(1986).
8. M.N.Bussac, R.Pellat, D.Edery, J.L.Soulé, Phys. Rev. Lett. 35, 1638, (1975).
9. B.Coppi, R.Galvao, R.Pellat, M.N.Rosenbluth, P.H.Rutherford, Sov. J. Plasma Physics 2, 533 (1976).
10. M.N.Bussac, D.Edery, R.Pellat, J.L.Soulé, in Plasma Physics and Controlled Nuclear Fusion Research (Proc. 6th Int. Conf. Berchtesgaden 1976), Vol 1, IAEA Vienna 607,(1977).
11. B.Basu, B.Coppi, Nucl. Fusion, 17,1245, (1977).
12. G.Ara , B.Basu, B.Coppi, G.Laval, M.N.Rosenbluth and B.V.Waddell, Ann. Phys. (N.Y.) 112 443,(1978).
13. R.E.Denton, J.F.Drake, R.G.Kleva, University of Maryland report UMLPF 86-004 (1985).
14. R.E.Denton, J.F. Drake, R.G.KLEVA, D.A.Boyd, Phys. Rev. Lett., 56, 2477 (1986).

15. J.W.Connor, R.J.Hastie, Culham Laboratory report CLM-M106 (1985).

16. L.E.Zakharov, Sov. J. Plasma Physics, 4, 503 (1978).

17. A.B.Mikhailovskii, Sov. J. Plasma Physics 9, 190 (1985).

18. L.A.Charlton, J.A.Holmes, H.R.Hicks, V.E.Lynch, and B.A.Carreras, Journal of Comp. Physics 63, 107 (1986).

19. T.C.Hender, R.J.Hastie, D.C.Robinson submitted to Nucl. Fusion.

20. K.McCormick, R.Bartiromo, H.S.Bosch, M.Brambillo, H.Derfler, A.Eberhagen, D.Eckhartt, G.Fussmann, O.Gehre, J.Gernhardt, G.v.Gierke, A.Giuliana, E.Glock, O.Gruber, G.Haas, M.Hesse, G.Janeschitz, F.Karger, M.Keilhacker, O.Klüber, M.Kornherr, P.B.Kotzé, M.Lenoci, F.Leuterer, G.Lisitano, H.M.Mayer, D.Meisel, V.Mertens, E.R.Müller, M.Münich, H.Murmann, H.Niedermeyer, W.Poschenrieder, H.Rapp, F.Ryter, K.H.Schmitter, F.Schneider, G.Siller, P.Smeulders, F.Söldner, K.H.Steuer, T.Vien, G.Vlases, F.Wagner, F.v.Woyna, M.Zouhar in Controlled Fusion and Plasma Physics (Proc. 12th European Conf., Budapest 1985) Vol 1, 199, (1985).

21. H.Soltwisch, W.Stodiek, A.Kaleck, J.Schlüter, U.S. DoE Report DoE/CH/03073-T26, 1985.

22. D.Edery, G.Laval, R.Pellat, J.L.Soulé, Phys. Fluids 19, 260, (1976).

23. I.B.Bernstein, E.A.Frieman, M.D.Kruskal, R.M.Kulsrud, Proc. Roy. Soc. A244 17 (1985).

24. A.H.Glasser, J.M.Greene, J.L.Johnson, Phys. of Fluids 18, 875, (1975).

25. J.A.Holmes, B.A.Carreras, H.R.Hicks, V.E.Lynch, K.E.Rothe, Phys. Fluids 25 800 (1982).

26. P.Kirby, F.Nave, J.A.Wesson, to be published in Plasma Physics and Controlled Nuclear Fusion Research (Proc. 11th Int. Conf., Kyoto, 1986).

27. G.L.Jahns, M.Soler, B.V.Waddell, J.D.Callen, H.R.Hicks, Nucl. Fus. 19 609, (1978).

28. D.J.Campbell, R.D.Gill, C.W.Gowers, J.A.Wesson, D.V.Bartlett, C.H.Best, S.Coda, A.E.Costley, A.Edwards, S.E.Kissell, R.M.Niestadt, H.W.Piekaar, R.Prentice, R.T.Ross, B.J.D.Tubbing, Nucl. Fus. 26 1085, (1986).

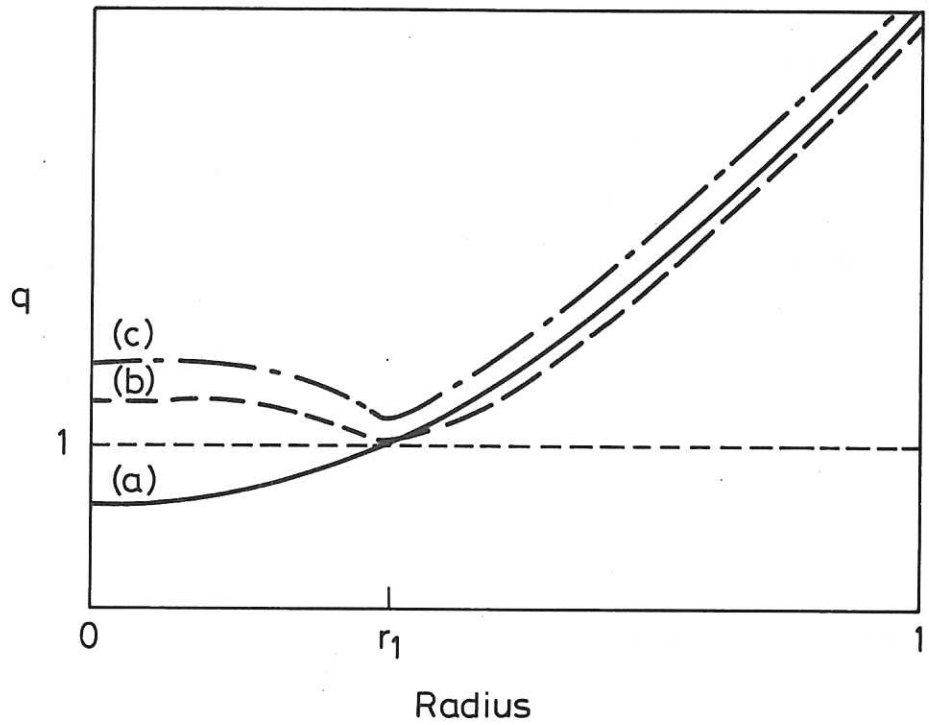

Fig. 1 Profiles of the safety factor $q(r)$ for which ideal mhd growth rates are calculated in eqs. (12), (13), and (14).

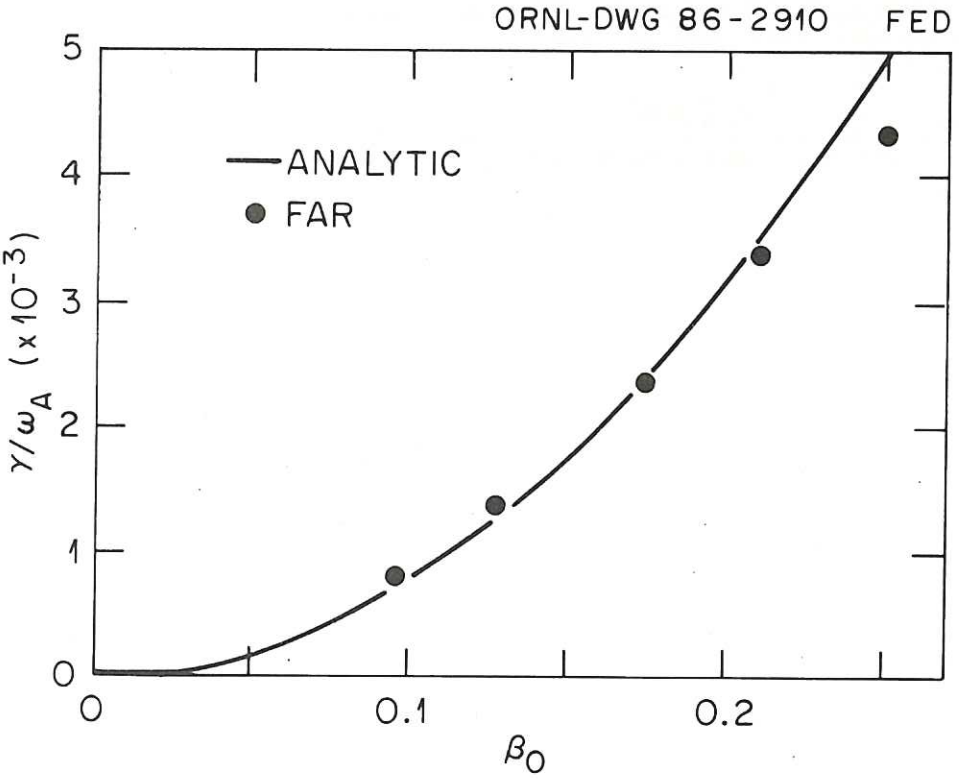

Fig. 2 Comparison of analytic growth rates (from equation (12)) and computed growth rates for the ideal mhd mode, as functions of peak $\beta_0 = \frac{2p(0)}{B_0^2}$.
Aspect ratio, $A = 10^2$, $q(r)=0.9(1+r^2)$, $p(r)=p_0(1-r^2)$.

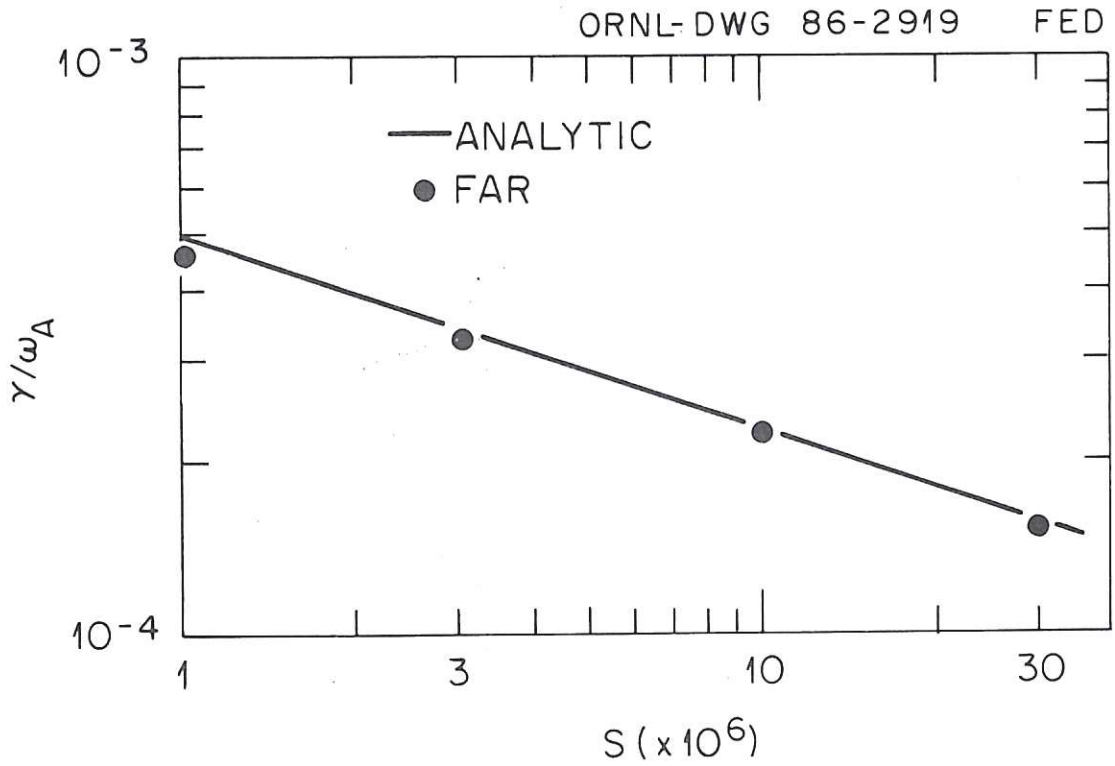

Fig. 3 Comparison of analytic [equation (20)] and computed growth rates for the resistive kink instability, as functions of magnetic Reynolds number S. $\beta_0 = 0$, $A = 10^2$, $q = 0.9(1 + r^2)$.

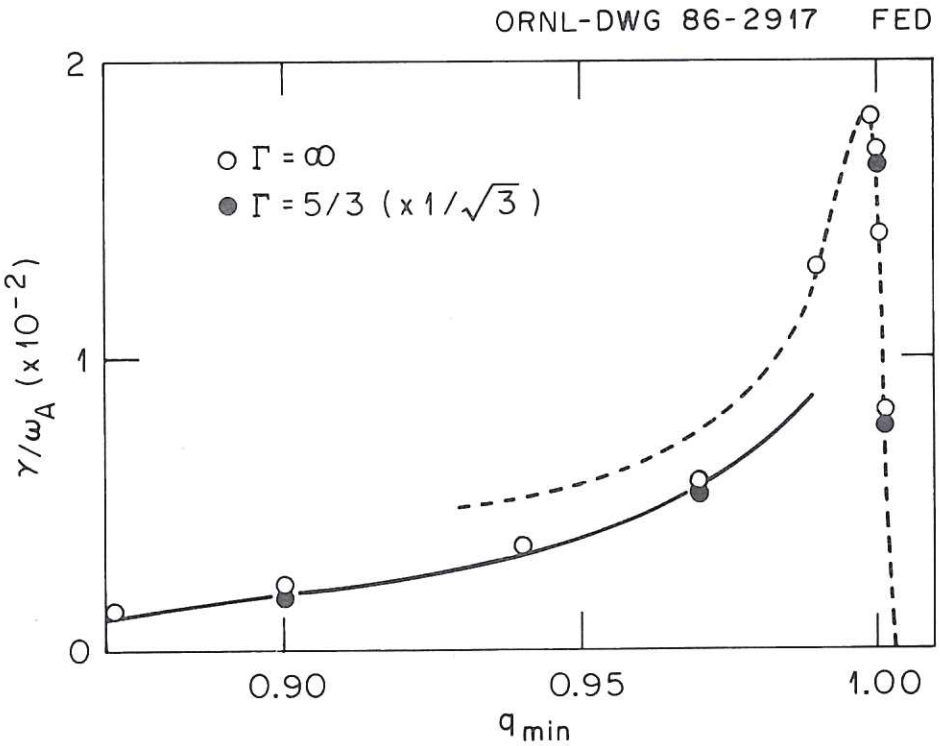

Fig. 4 Comparison of analytic and computed ideal growth rates for the non-monotonic safety factor $q(r) = q_{min} + 0.2(1-4r^2)^2$, plotted against minimum value of q. The broken curve is calculated from eq.(14) (appropriate for a single inertial layer) the solid curve from eq.(24) (appropriate for two distinct layers). Solid circles were computed using the compressible FAR code (and corrected by the factor $1/\sqrt{3}$, see text). Circles were computed using the incompressible code. $A = 10$ and $\beta_0 = 0$.

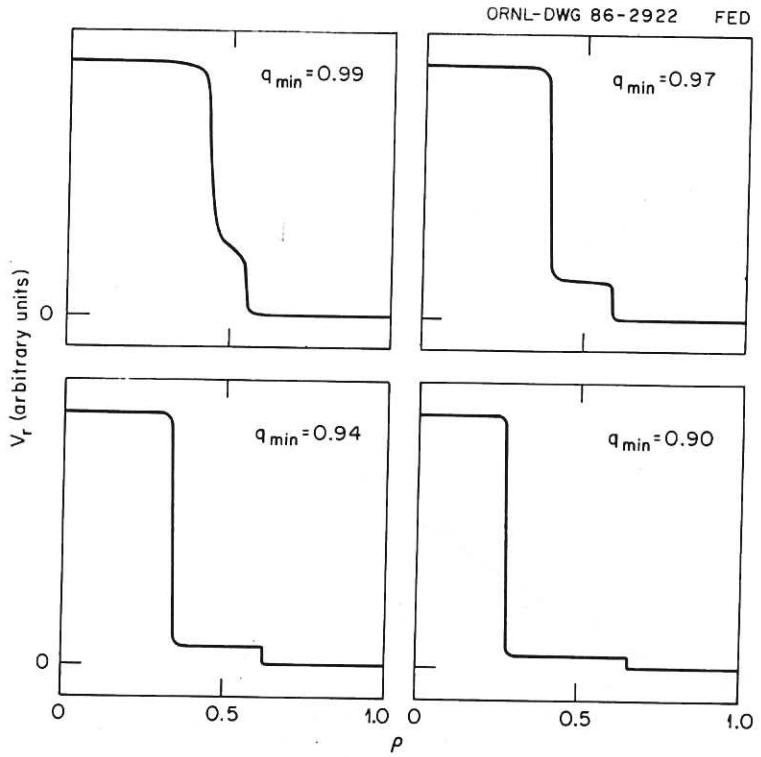

Fig. 5 Structure of the eigenfunction ($m=1$ component of radial velocity) as a function of radius, for various values of q_{min}. $\beta_0=0$; $A=10$; $q=q_{min}+0.2(1-4r^2)^2$.

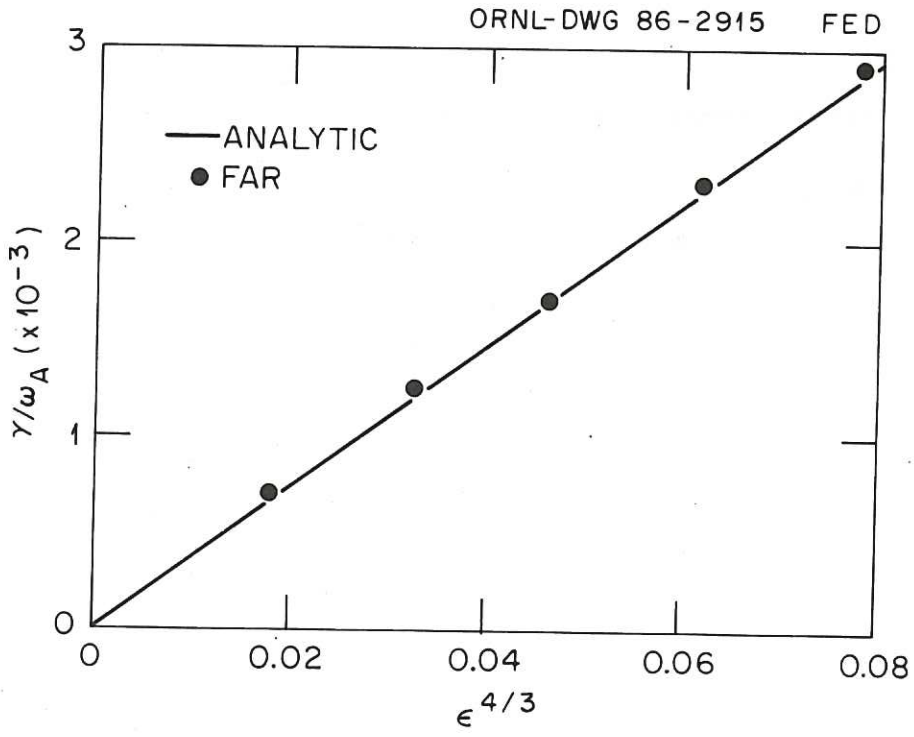

Fig. 6 Ideal growth rate against inverse aspect radio $\epsilon=A^{-1}$, for the same equilibrium as Figs.4, 5. $q_{min}=1.0$. Analytic results (solid curve) are from eq.(13).

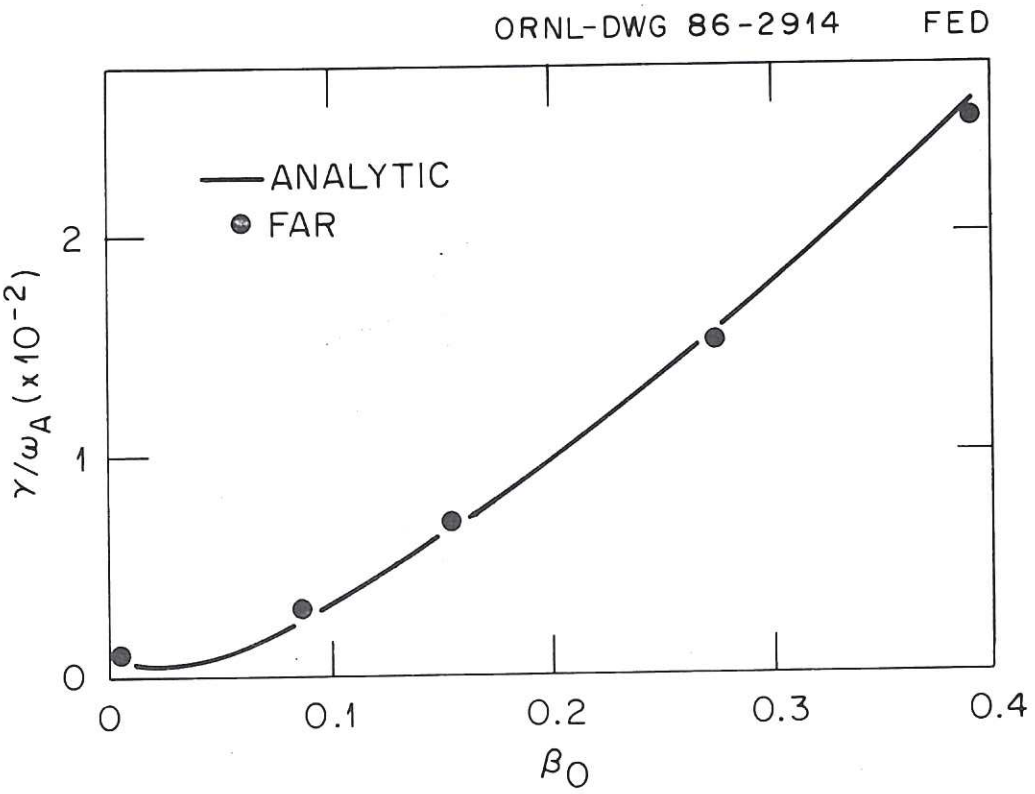

Fig. 7 Growth rate plotted against, β_0, peak value of beta. Analytic results (solid line) are from eq.(13). $A=10$, $q=1+0.1(1-9r^2)^2$, $p=p_0\left(1-\frac{\psi}{\psi_a}\right)^2$ with $\psi=\int_0^r R_0 B\theta\, dr$.

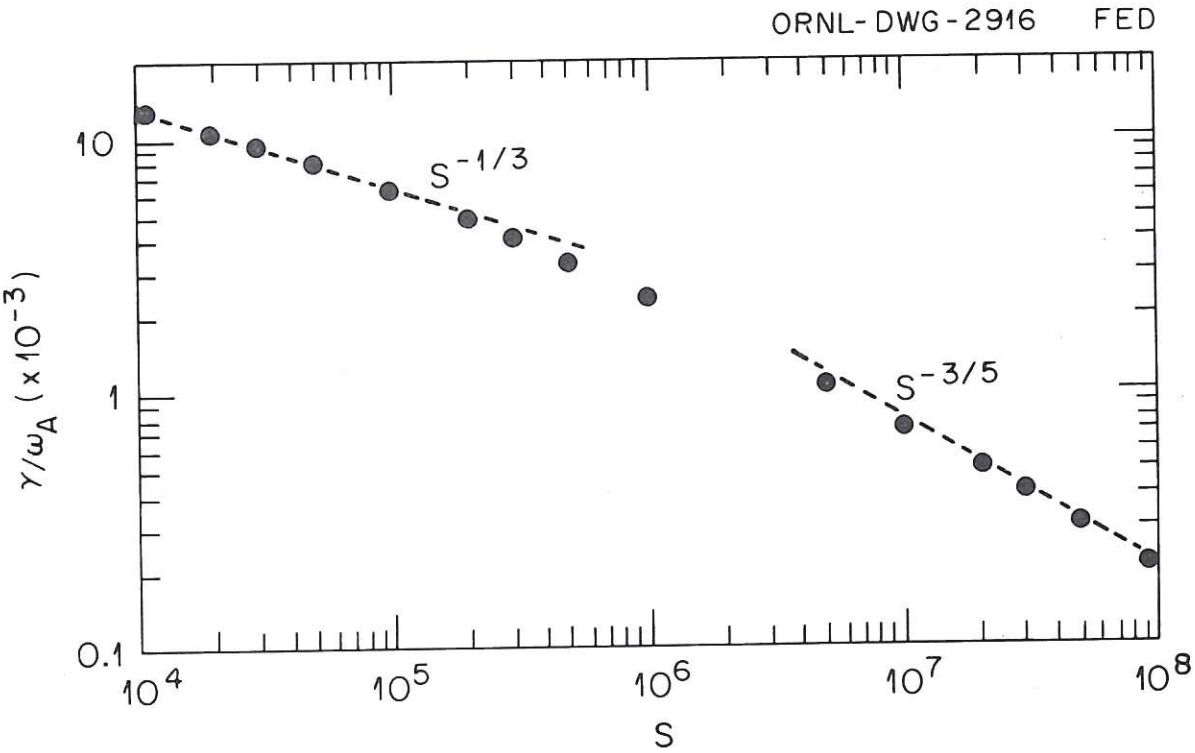

Fig. 8 Computed growth rate of $m=1$ kink mode as a function of magnetic Reynolds number S, $A=1.4$, $q=0.9\left(1+\left(\frac{r}{0.65}\right)^4\right)^{1/2}$, $\beta_0=0$.

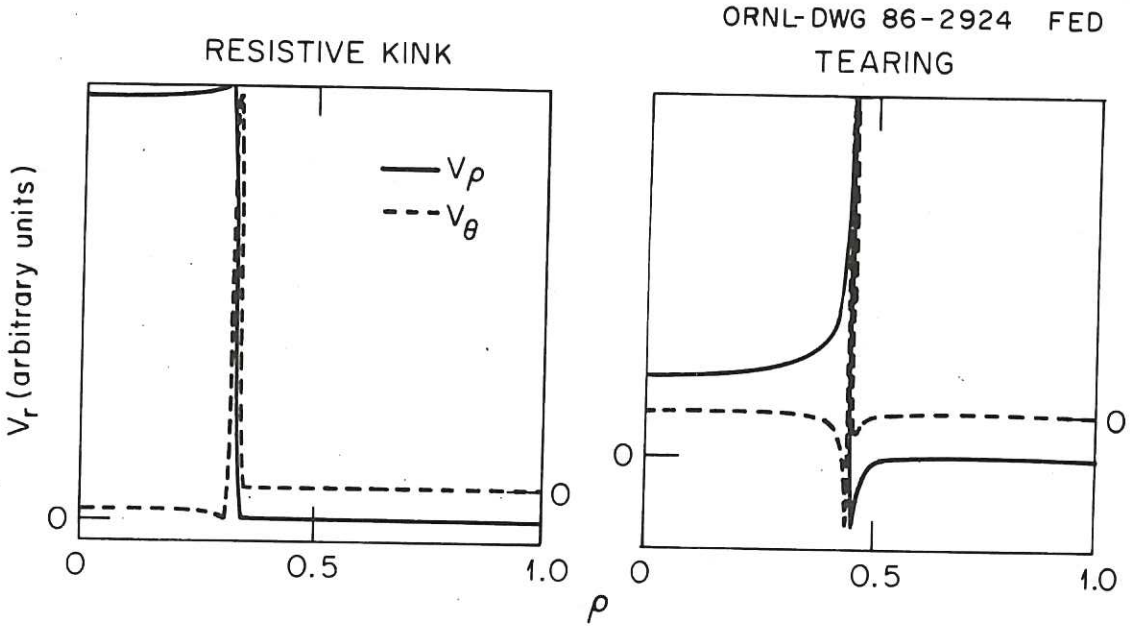

Fig. 9 Eigenfunction $V_r(r)$ for the resistive kink mode ($A=10^2$, $\beta_0=0$, $q=0.9(1+r^{2)}$, $S=10^7$) and $m=1$ reconnecting mode $\left(A=1.4,\ \beta_0=0,\ q=0.9\left[1+\left(\frac{r}{0.65}\right)^4\right]^{1/2},\ S=10^7\right)$.

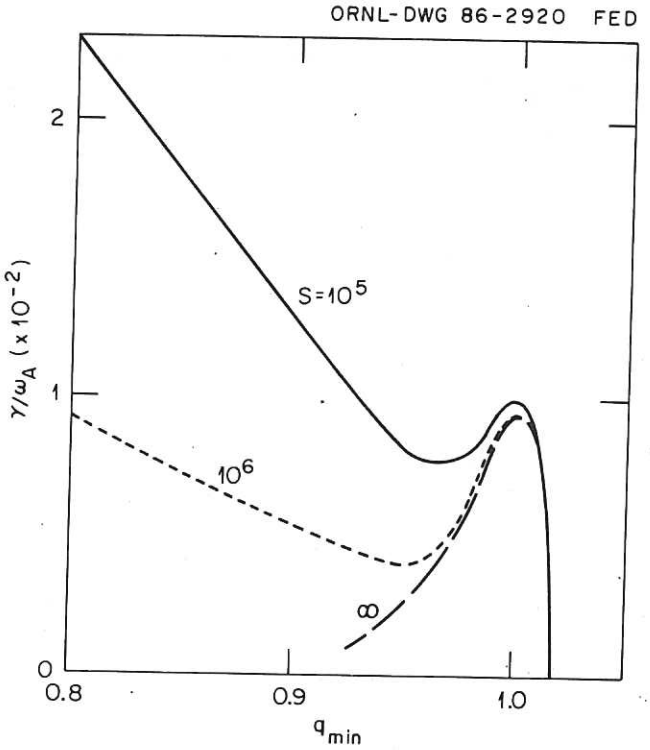

Fig. 10 Computed growth rates for $A=2.5$ $q(r)=q_{min}+0.1(1-8r^2+16r^4)$, $\beta_0=0$ and several values of S, plotted against q_{min}.

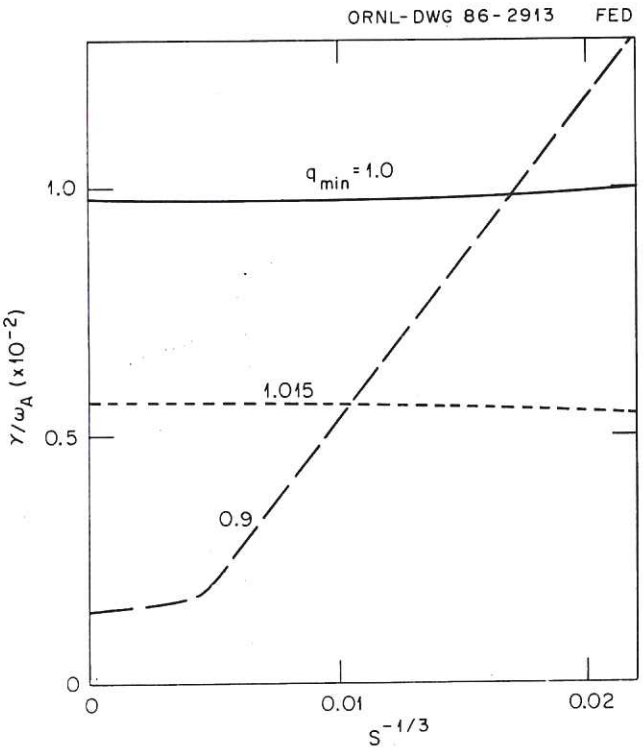

Fig. 11 Computed scaling of kink mode growth rates with S. for three values of q_{min}. Same equilibrium as for Fig. 10.

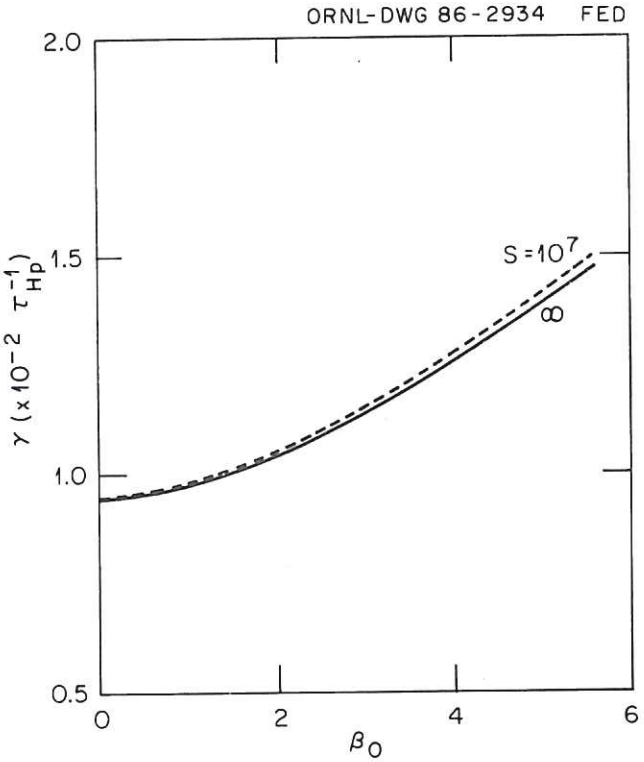

Fig. 12 Computed growth rate as a function of β_0. Same equilibrium as Figs 10, 11, with $q_{min}=1.0$.

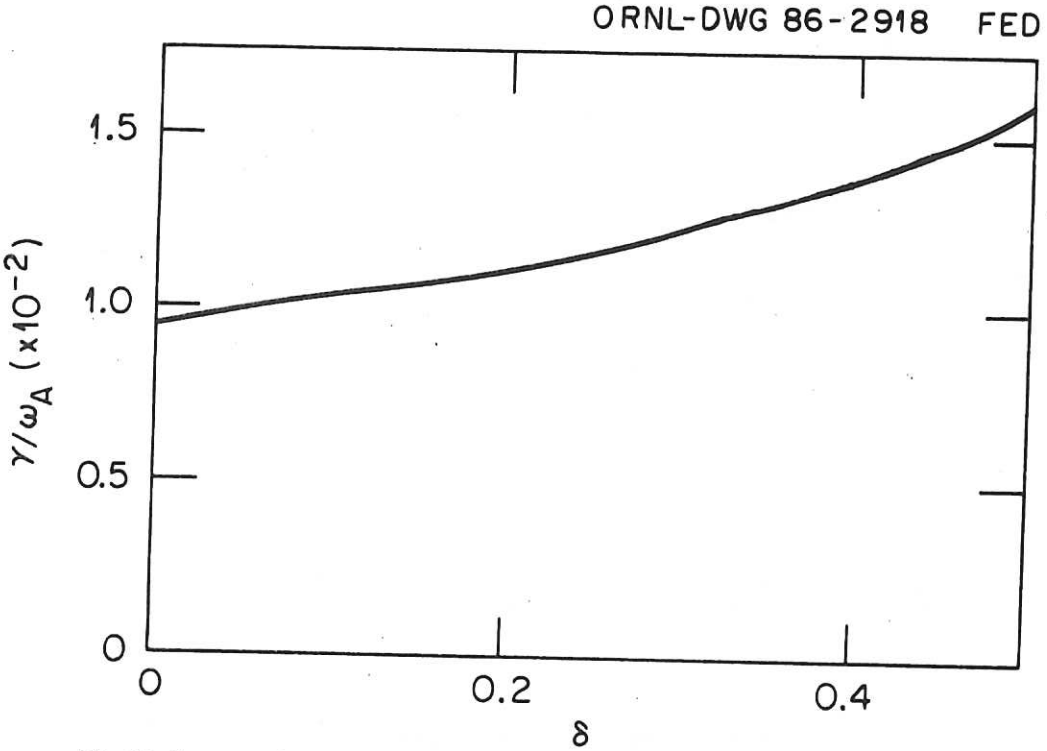

Fig. 13 Computed growth rate as a function of triangularity of the plasma boundary. Equilibrium of Fig. 10 with $\beta_0 = 0$, $q_{min} = 1.0$.

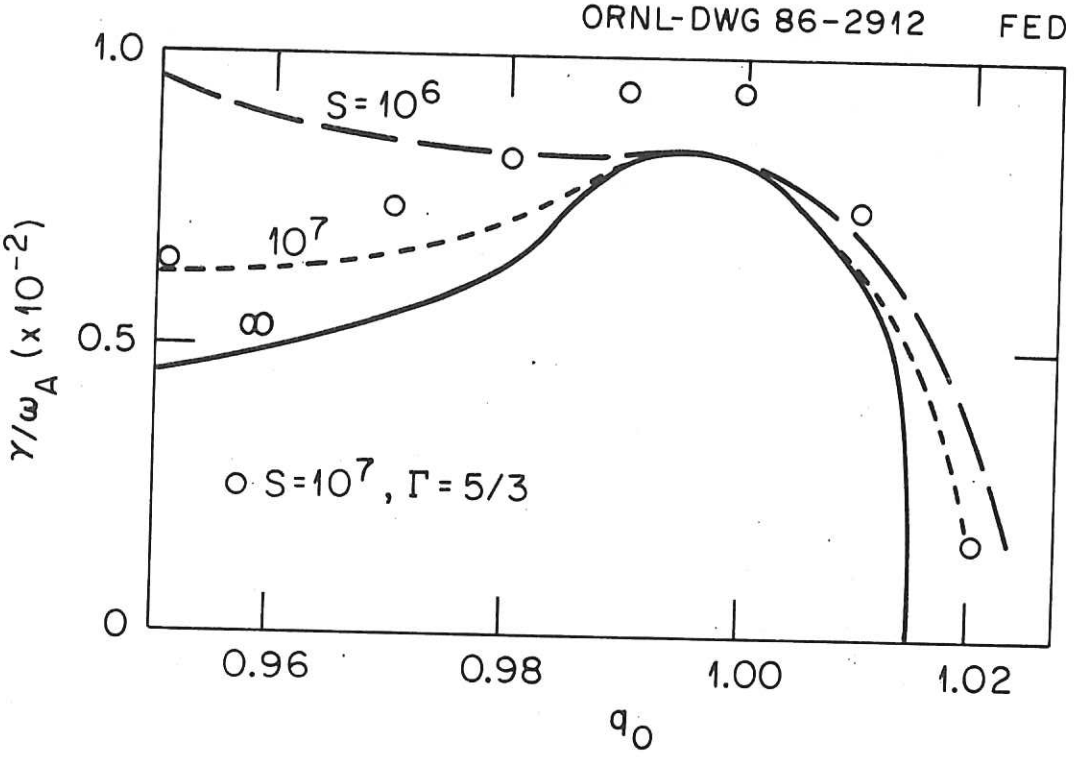

Fig. 14 Computed growth rate as a function of q_0, for $A = 2.5$, $q = q_0\left(1 + \left(\frac{r}{0.462}\right)^{12}\right)^{1/6}$, $\beta_0 = 2\%$, $p(r) = p_0\left(1 - \frac{\psi}{\psi_a}\right)^2$, and for various values of S. Open circles are growth rates obtained using the compressible FAR code at $S = 10^7$.

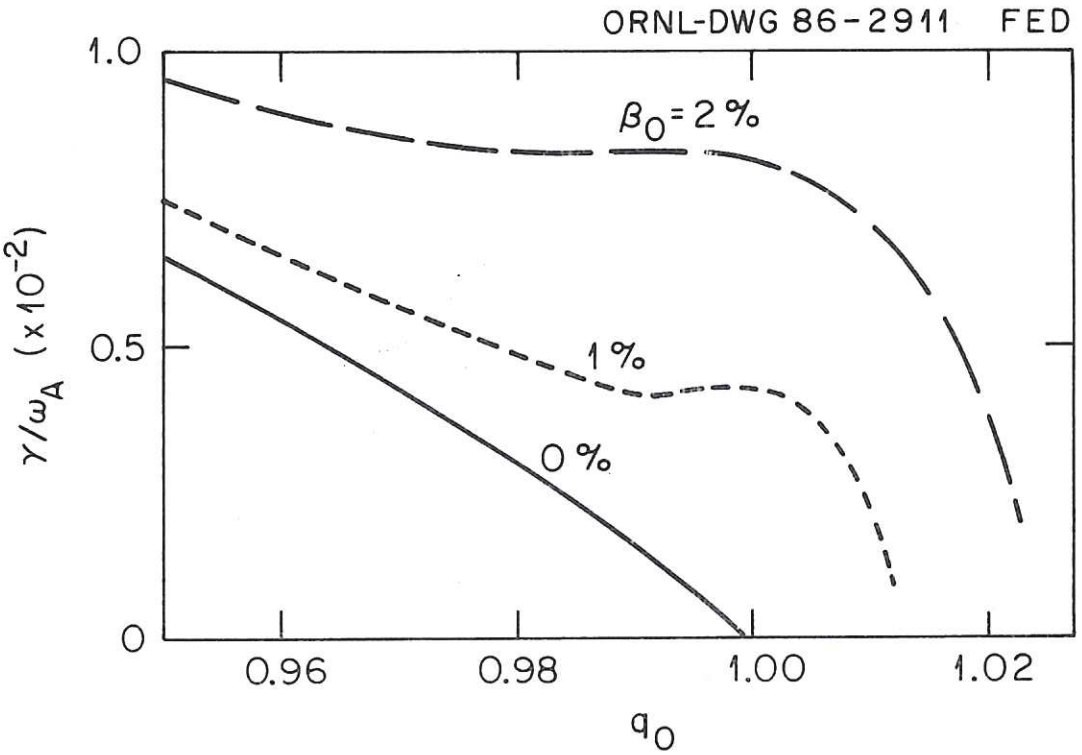

Fig. 15 Computed growth rate as a function of q_0 for various values of β_0. Same equilibrium as Fig. 14 $S=10^6$.

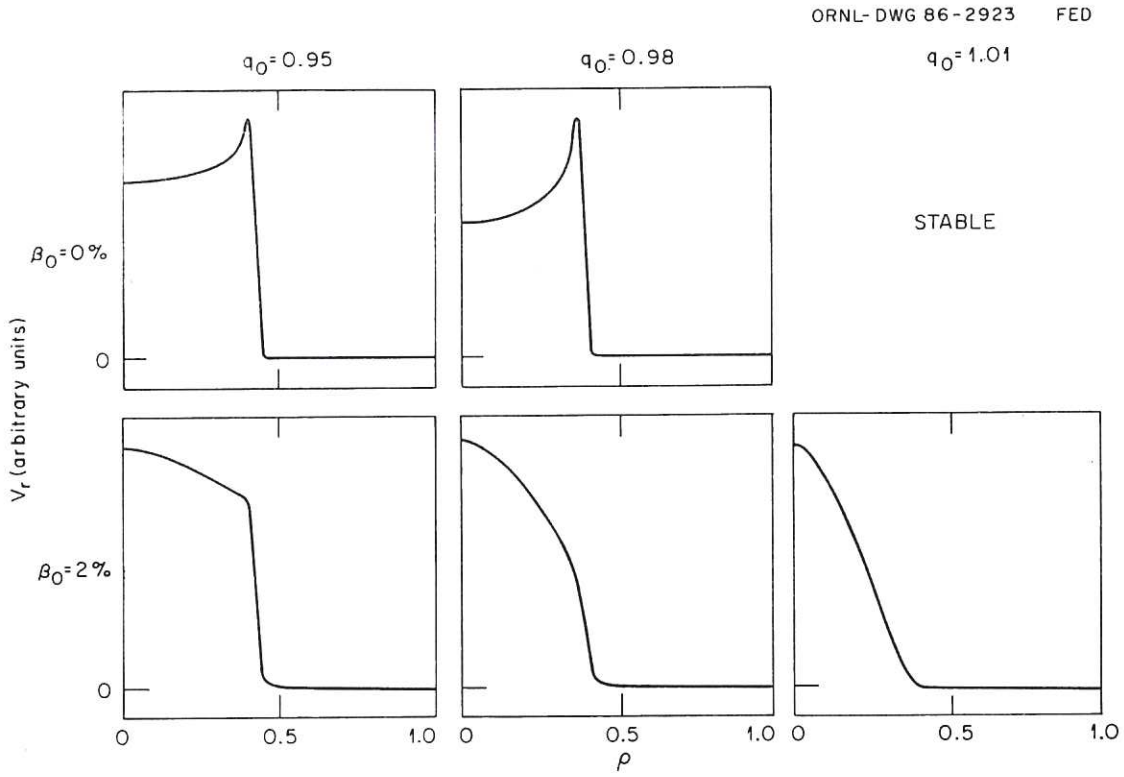

Fig. 16 Comparison of $m=1$ eigenfunction, $V_r(r)$ for various β_0, q_0. Same equilibrium as Fig. 14 $S=10^6$.

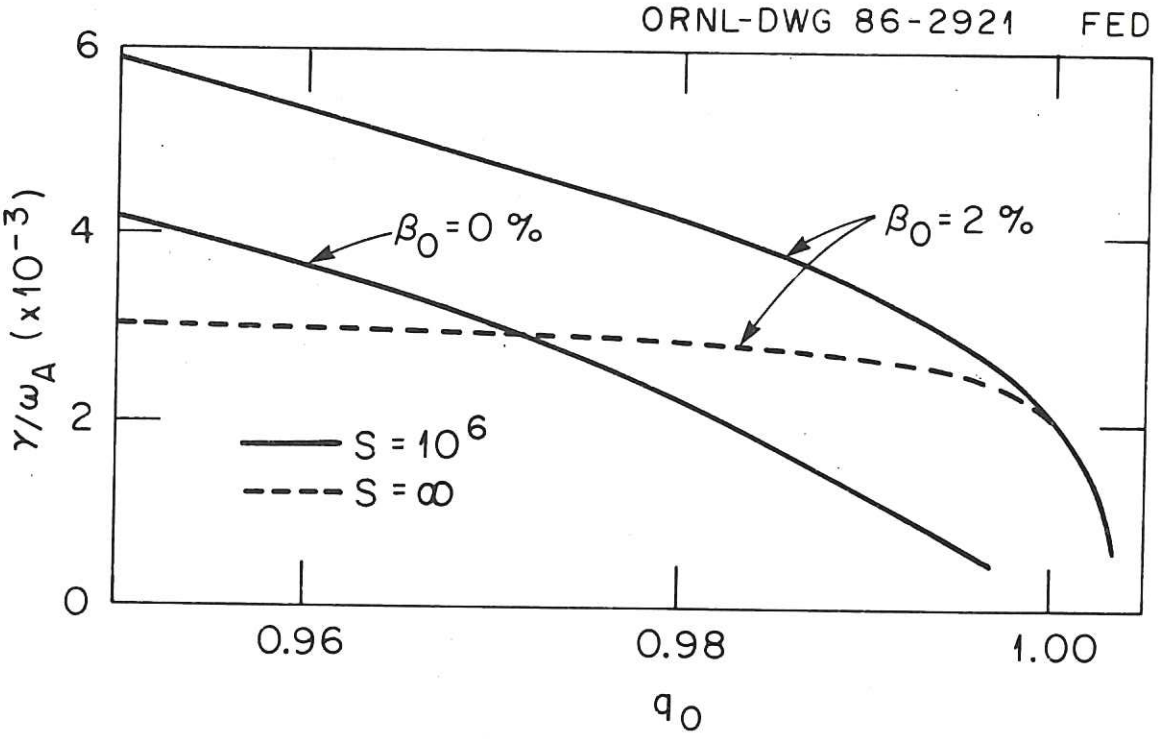

Fig. 17 Computed growth rates of $m=1$ kink mode for $q(r)=q_0\left(1+\left(\frac{r}{0.46}\right)^4\right)^{1/2}$, $A=2.5$, $p=p_0\left(1-\frac{\psi}{\psi_a}\right)^2$ and various values of β_0 and S.

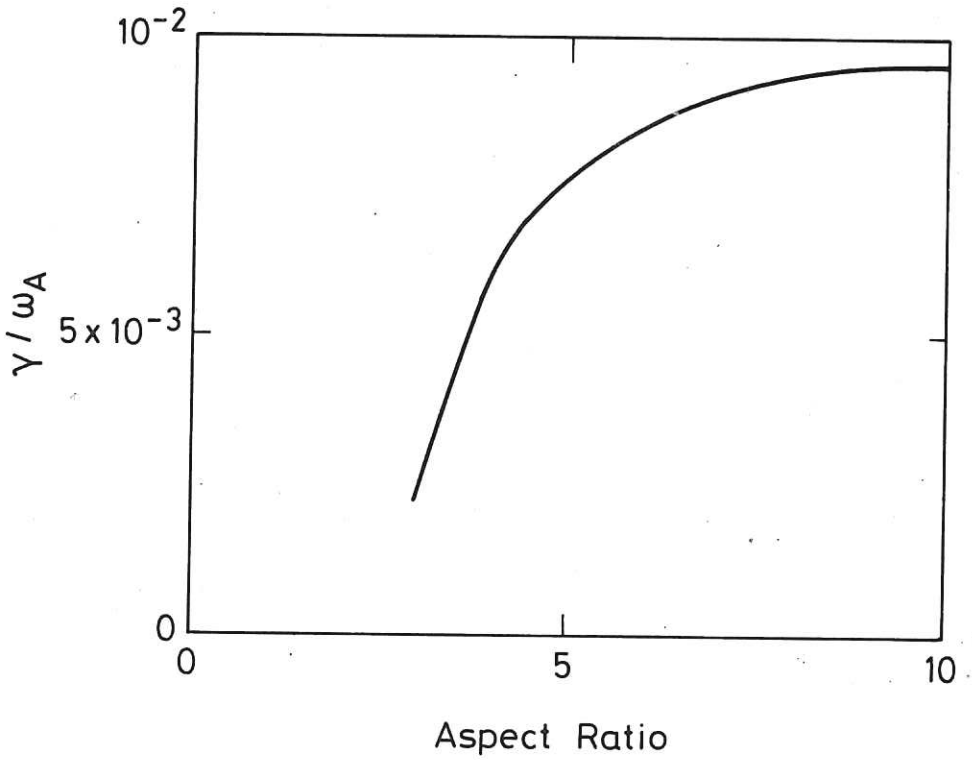

Fig. 18 Computed growth rate of $m=1$ kink mode for $q(r)=0.6+2.2r^2-2.2(r^2-r_1^2)e^{-100(r^2-r_1^2)}$, $r_1=0.426$, $\beta_0=0$, $S=10^5$, plotted against aspect ratio A. The mode becomes overstable at the smallest aspect ratio shown.